International Journal of Solids and Structures 264 (2023) 112118

Contents lists available at ScienceDirect

International Journal of Solids and Structures

journal homepage: www.elsevier.com/locate/ijsolstr

Guided Double Cantilever Beam test method for intermediate and high loading rates in composites

S.A. Medina [a,*], E.V. González [a], N. Blanco [a], J. Pernas-Sánchez [b], J.A. Artero-Guerrero [b]

[a] AMADE - Analysis and Advanced Materials for Structural Design, Polytechnic School, Universitat de Girona, Carrer de Maria Aurèlia Capmany i Farnés, 61, 17003 Girona, Spain

[b] Department of Continuum Mechanics and Structural Analysis, Universidad Carlos III de Madrid, Leganés, Madrid, Spain

ARTICLE INFO

Keywords:
Mechanical testing
Fracture toughness
Polymer-matrix composites (PMCs)
High loading rates

ABSTRACT

Although the rate-dependent behaviour of the interlaminar fracture toughness of fibre reinforced composites has been a matter of ongoing research in recent decades, further research is required into characterising these properties and, consequently, developing more reliable constitutive models to simulate dynamic events. Furthermore, despite the various studies that have been carried out, no consensus on which test method to use to characterise these properties has yet been reached. This paper presents a new test method for measuring the dynamic mode I interlaminar fracture toughness in composite laminates by using a novel device based on a modified Double Cantilever Beam test method with a guided tensile configuration. In contrast to other methods reported in the literature, the proposed device guarantees a symmetric crack opening and, thus, pure mode I propagation during high loading rate testing. When used in a dynamic servo-hydraulic testing machine with controllable displacement rate, a constant opening velocity can be achieved. The Guided Double Cantilever Beam testing method is validated against a quasi-static Double Cantilever Beam test, showing good agreement between the results. The testing method has been satisfactorily tested under intermediate/high loading rates, from 0.1 to 10 m/s.

1. Introduction

The use of composite materials for structural applications in a number of industries has experienced a significant increase in recent years thanks to being able to provide new solutions for engineering applications. However, further improvement in the knowledge of the mechanical behaviour of these materials under dynamic conditions at different strain rates is required if more accurate and reliable designs are to be achieved. Different methods have been developed to predict and study the dynamic behaviour of composite structures. For instance, Finite Element (FE) simulation tools are one of the main design methodologies employed for composite structures. The accuracy of the FE predictions relies, in part, on the material properties and the constitutive laws implemented. Generally, the material properties required for numerical analysis are characterised under quasi-static loading conditions (May, 2016), however, these properties are usually used to feed the constitutive models for the dynamic simulation of a given structure. Therefore, suitable test methods need to be developed that can obtain reliable input data for the material models used for dynamic loading. Using rate-dependent material models has been demonstrated to significantly influence the numerical prediction of the structure behaviour (Neumayer, 2017) in, for instance, crash and impact simulations (May, 2015).

In addition, diverse experimental test set-ups have evidenced the different strain rate dependencies of key properties such as stiffness and strength, even for the same material and conditions (Jacob et al., 2005). These differences in the values obtained are basically due to the data reduction method applied, the different test set-ups that can be used, and the fact that measuring reliable forces and crack growths at high strain rates is challenging. Most of the test set-ups for high strain rates derive from quasi-static test methods, despite being inappropriate because different phenomena (mainly dynamic effects) are present.

One of the main concerns about composite structures is their weakness against the delamination of individual plies. One of the material properties required for the numerical analysis relative to delamination is the interlaminar mode I fracture toughness. This material property in composite materials has been extensively studied under quasi-static loading conditions (Sela and Ishai, 1989; Brunner et al., 2001; Nasuha et al., 2017; Siddique et al., 2021), most commonly using the Double Cantilever Beam (DCB) test. Different standards have been defined

* Corresponding author.
E-mail address: sergio.medina@udg.edu (S.A. Medina).

https://doi.org/10.1016/j.ijsolstr.2023.112118
Received 29 June 2022; Received in revised form 17 November 2022; Accepted 5 January 2023
Available online 10 January 2023

for the quasi-static mode I interlaminar testing of FRPs (Fibre Reinforced Polymers), such as ISO 15024:2001 (2001), ASTM D5528-13 (2013) and JIS K 7086:1993 (1993). For dynamic loading cases, the information available about the behaviour of polymer-based composite materials is limited. Strain rate effects on the mode I, mode II, and mixed mode (I/II) fracture toughness properties of FRP composites were summarised in the works of Jacob et al. (2005), and Cantwell and Blyton (1999), who demonstrated that the strain rate effect acts on the matrix properties, affecting fracture toughness. As Jadhav (2003) specified in his work, delamination and matrix cracking are the principal modes of composite specimen failure when dynamically loaded out of the plane, which agrees with previously reported behaviour (Jacob et al., 2005; Cantwell and Blyton, 1999).

Whilst there seems to be consensus to determine the rate-dependent in-plane properties (Körber, 2010), measuring rate-dependent fracture toughness in composite materials, for instance pure mode I delamination, is still open to question. Unlike for quasi-static loading, no protocols or standard test methods have yet been defined. Since 2004, the ESIS TC4 committee has made some efforts to implement a testing protocol to determine mode I interlaminar fracture toughness for unidirectional FRP composites at moderately high loading rates (~ 1 m/s) (Brunner et al., 2021). However, from the studies available in the literature, it can be concluded that there is no agreement on the trend of fracture toughness with regard to loading rate. In some cases, an increase in the mode I fracture toughness was noted with an increase of the loading rate (Colin de Verdiere et al., 2012a; Aliyu and Daniel, 1985; Feng et al., 1983; Tsai et al., 2001), or, likewise, a decrease in the mode I fracture toughness with an increase in the loading rate (Kusaka et al., 1998; Mall et al., 1987; Marzi et al., 2014; Smiley and Pipes, 1987). That said, in other studies no effect was observed (Colin de Verdiere et al., 2012b; Blackman et al., 1995, 1996; Sun and Han, 2004). For example, Aliyu and Daniel (1985) reported an increasing fracture toughness when increasing loading-rates in AS4/3501-6 carbon composite laminates, while Smiley and Pipes (1987) reported the opposite trend for the same material using the same DCB test method.

In recent decades, several test set-ups have been proposed. The review of May (2016) presents a description of the different test configurations and specimens proposed to assess mode I dynamic interlaminar fracture toughness in terms of the strain or loading rates. Jiang and Vecchio (2009) also reviewed dynamic fracture toughness tests using the Hopkinson Bar apparatus for different materials, including composites. Even so, the DCB test (ISO 15024:2001, 2001) is the most commonly adopted set-up for analysing the dynamic fracture toughness of composites in mode I loading. The test set-ups reported in the literature encompass a wide range of loading and boundary conditions, including screw driven (Low et al., 2019) or hydraulic test machines, modified Charpy and Izod impact tests, drop weight impact tower (Thorsson et al., 2018) and Hopkinson bar apparatus (Isakov et al., 2019).

Blackman et al. (1995, 1996) used a DCB specimen in a servo-hydraulic testing machine under high loading rates. The main drawback of this method is that under high loading rates the deformation of the two arms of the specimen is no longer symmetric. Thus, it becomes a mixed mode test and a mode I analysis cannot longer be used. Moreover, unstable crack growth was evidenced. Other authors had the same issue with the symmetry of the DCB test under high loading rates (Colin de Verdiere et al., 2012b; Blackman et al., 2009).

To solve the issue of the symmetrical opening, Hug et al. (2006) defined a complex device, based on the DCB test method, to amplify the quasi-static loads. However, due to the inertia effect of the fixture, the loading rate was limited to 1.6 m/s. Thereafter, some authors used an internal wedge test (wedge-insert inside the DCB specimen), where crack length is almost constant during the test, yielding to crack growth stabilisation and opening symmetry (Kusaka et al., 1998; Isakov et al., 2019; Dillard et al., 2011; Oshima et al., 2018a). The drawback of this test method is the friction between the crack surfaces and the wedge while it is being driven between the two arms; and which is complex to measure. Additionally, new proposals based on an external wedge falling method for a DCB specimen in a drop weight tower were developed, allowing for a symmetrical opening of the specimen (Thorsson et al., 2018; Xu and Dillard, 2003; Yamagata et al., 2017; Riezzo et al., 2018; Oshima et al., 2018b), and removing the surface-to-surface friction between the wedge and the crack surfaces by using two external loading blocks. The loading method is, however, not free of friction, due to contact between the rollers and the wedges as well as the bearing blocks. The authors managed to minimise the friction by employing smooth wedge surfaces and tight tolerance machining and lubrication. In spite of that, the load is of an impact nature without constant opening velocity and unstable crack growth when using a drop tower machine. Liu et al. (2019) proposed a symmetrically opened DCB test for high loading rates using a dual electromagnetic Hopkinson bar system, thus solving the issues of the friction between the crack surfaces and the wedge, but limited to the use of this particular test device.

Another issue associated with testing at high rates is related to the appropriate measuring of the applied load; so that it can then be used as an input for the data reduction. Typically, the load measured in such situations oscillates with significant amplitudes at high frequencies due to the dynamic effects (Colin de Verdiere et al., 2012b; Blackman et al., 1995, 2009) and these cannot be filtered because it is not clear which oscillations are spurious and which are not. Therefore, the signal from the load cell cannot be considered as representative of the material response and a load-independent data reduction approach is needed. Additionally, special care must also be taken when the displacement is recorded. The values of displacement can be affected by dynamic accelerations and oscillation effects. Blackman et al. (1995) compared the displacement recorded through the test machine and the one monitored by high-speed photography and found that the response is the same at low testing rates, whereas at high testing rates it is underestimated.

The measurement of the crack tip during propagation, as required for the data reduction, is also a key aspect for these type of tests. Usually, crack tip propagation is measured optically using high-speed cameras, thus requiring the set-up to be designed in such a way that crack propagation and loading-point opening, at least, can be graphically recorded.

This paper presents a test method, the Guided Double Cantilever Beam (GDCB), to measure mode I interlaminar fracture toughness in composites laminates under intermediate/high loading rates using a novel device. The proposed tool is based on a modified DCB test method with a guided tensile configuration. One of the main characteristics of the device, in contrast to other methods reported in the literature, is that it allows for a symmetric opening of the specimen arms and reaches a constant opening velocity at the loading points. The tool presents a system of grips for clamping the specimen and allowing the load/displacement transmission from the main part of the tool. It includes a simple, fast and reliable design avoiding adhesive joints and overcomes the problems associated to end blocks and piano hinges. A validation of the test method is conducted by comparing the quasi-static mode I fracture toughness obtained with the GDCB method and the standardised quasi-static mode I fracture toughness ISO 15024. A test campaign under intermediate and high loading rates is also carried out, showing a good performance of the tool at these velocities. The device for the GDCB testing has been patented with international application number PCT/ES2021/070415 and publication number WO/2022/003219.

2. Proposed test method

The test method proposed in this work is designed for applying a symmetric opening to a DCB type specimen under a controlled displacement rate to determine the dynamic interlaminar fracture toughness of composites under pure mode I loading. The system is designed to apply intermediate and high loading rates using a high-speed testing

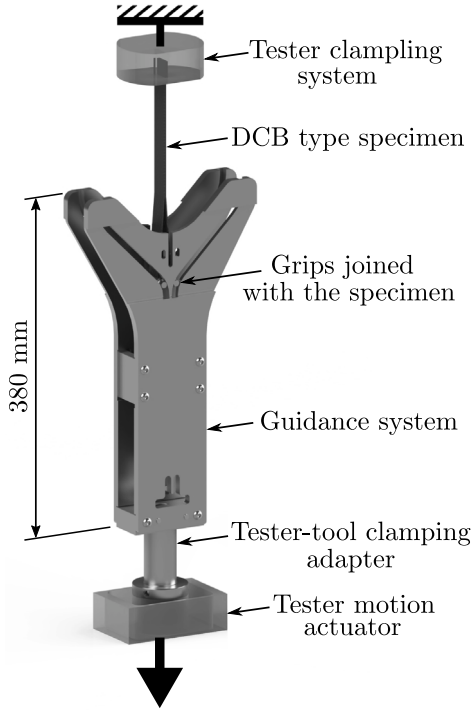

Fig. 1. GDCB tool for the intermediate/high loading rates testing.

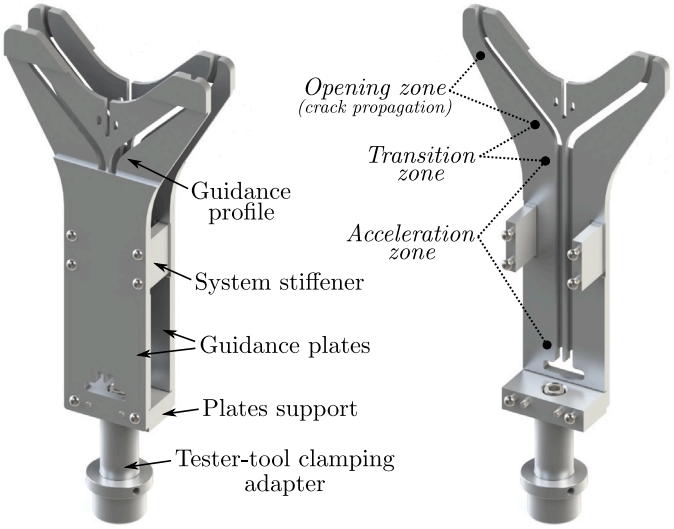

Fig. 2. Guidance system of the GDCB tool.

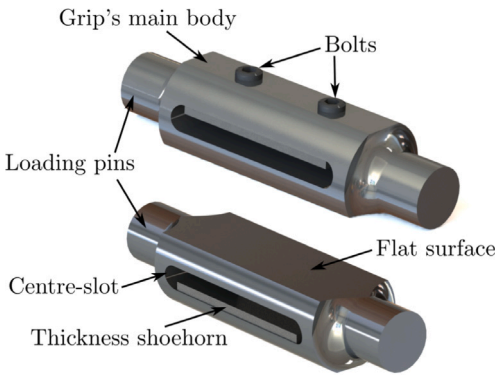

Fig. 3. GDCB grips.

machine. Fig. 1 shows the tool designed for the GDCB test method. The tool drives the opening of a DCB specimen using guiding plates and by applying a tensile load. Additionally, it offers the possibility to reach higher opening velocities than those applied by the machine, i.e., with an increment around two and a half times the displacement rate of the tester.

The device has been designed to be used preferably in hydraulic high strain-rate testing machines, this allowing the test velocity to be controlled to obtain a constant opening velocity. To maintain the configuration of the machine's inertia, and other related settings, the proposed tool has a similar mass to the manufacturer's tool commonly used in the Instron VHS servo-hydraulic high loading rate machine for tensile testing. The tool can also be used in other testing machines (such as the drop tower apparatus) with its adaptor for clamping purposes. However, in order to achieve constant velocity during propagation, use in hydraulic high strain-rate testing machines is preferred.

2.1. Tool parts

The GDCB testing device is composed of two separated parts. The first is the guidance system (as seen in Fig. 2) and includes a set of two plates with a guidance profile, a support that joins the guidance profile plates and keeps them parallel to each other, two plates that join the two guidance plates and offer stiffness to the set, a cylindrical adapter for clamping the device to the testing machine (external to the testing tool) and the corresponding screws and pins required.

The second part of the device corresponds to the one that transfers the load from the guidance system to the specimen (see Fig. 3). It is composed of a set of two grips clamped to the end of each of the symmetrical arms of the test specimen. Each grip consists of a main metallic body with a prismatic centre-slot where one of the arms of the specimen is clamped using a metallic plate or thickness shoehorn and two tightening bolts. Two round and stiff ends are machined in the main body of the grip to act as loading pins at the opposite ends. The grips are designed to enforce the loading point in the neutral axis of the specimen arms, avoiding the non-linear effects due to the rotation of the loading blocks. Likewise, the distance between the load application point and the edge of the grip has been defined as short as possible to minimise the stiffening effect on the specimen while ensuring the correct transmission of forces. As all the interconnections of the different parts of the device are mechanical, there is no need for gluing clamps, thus allowing for easy reuse of the system to test DCB specimens with common thicknesses.

The tool has been designed in such a way that it allows for the displacements and crack propagation to be measured via image analysis using optical tracking, therefore using a data reduction method based on displacements only. Even so, if desired, the tool allows for measuring the load through the load cell or other techniques.

2.2. Tool operation

As shown in Fig. 1 for a vertical configuration of the system (it can be also mounted in other directions depending on the testing machine), the specimen is held by the clamping grips of the machine and loaded by applying a single tensile displacement to the cylindrical tester-tool clamping adapter of the guidance system. The transfer of the opening load to the specimen involves friction in the contact between the guides and the pins of the grips. However, this friction can be minimised by means of smooth surfaces and bearing-like movement ensured by tight tolerances and good lubrication. In any case, the friction coefficient between the load pins and the guides can be considered as small and

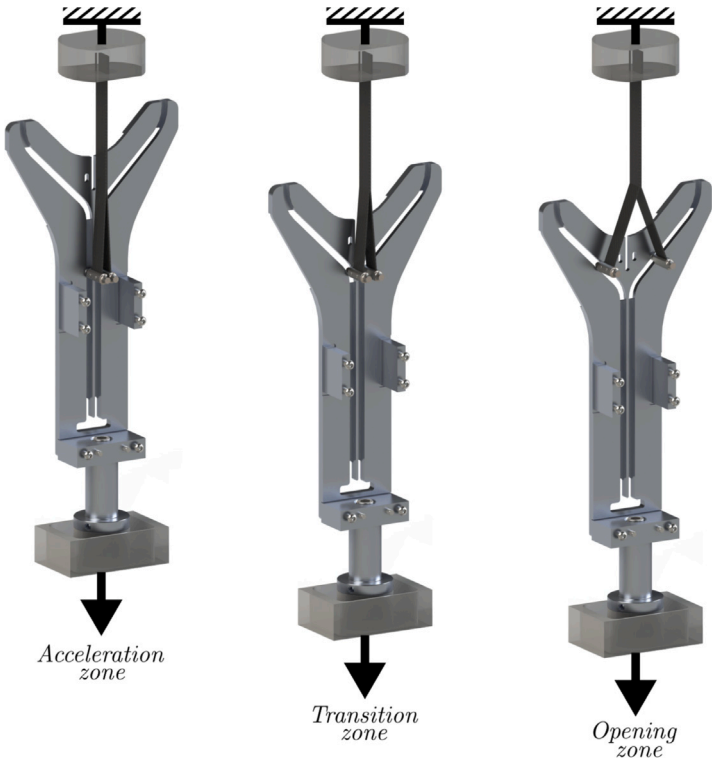

Fig. 4. Opening process of the specimen during a test (from left to right).

constant, contrary to what can happen in the case of the internal-wedge-driven test, where the coefficient of friction changes from the initial crack zone to the newly generated surface.

When the guidance system is pulled away in the tensile direction of the specimen, the guidance profiles in the guidance plates steer the pins of the grips resulting in an opening displacement of the specimen arms. The guidance profiles contain an acceleration zone where no opening displacement of the specimen arms is achieved to allow for the system to accelerate without the arms opening until the constant speed value desired is reached, as shown in Fig. 4. Next, the pins are driven to a transition zone to switch from the acceleration movement with no opening displacement, to the opening zone where the constant opening displacement is applied. The transition zone is designed to avoid sudden changes in the acceleration of the grip pins, thus the initiation of the crack propagation starts only when the constant velocity of the machine is reached and after the transition zone, i.e., where the opening velocity is constant (see Fig. 4). The guidance profile angle in the opening zone can be varied. In this study, a 45° guiding angle, with respect to the machine's movement, was chosen so that the opening and axial loading on the pin are of equal magnitude. The test device is complemented with an extra mounting tool to put together and correctly align the grips on the specimen before testing. In this way, when the specimen is clamped to the testing machine, the correct alignment between the machine, the guiding-plates, and the specimen is guaranteed and, consequently, a symmetrical opening is achieved.

The system has been designed in such a way that the specimens to be used are similar to those defined for characterising mode I interlaminar fracture toughness in laminated materials, i.e., the DCB test (ISO 15024:2001, 2001). However, some changes regarding the initial crack length and the length of the specimen are recommended to ensure crack propagation within the opening zone (see Section 3.1).

As mentioned before, besides the opening force, the GDCB method involves an additional axial force in the specimen arms that will load both arms in tension and, in turn, generates a flexural moment that will induce bending energy. Although the contribution of this axial force is smaller than that of the opening forces, it must be taken into account if the fracture toughness of the material is to be determined correctly (see Section 2.3). The developed tool uses a set of external guiding profiles in a tensile configuration because composite materials usually behave better under tension than in compression. In this way, this design avoids impacts in the specimen such as those encountered when using the falling external wedge method (Thorsson et al., 2018; Xu and Dillard, 2003; Yamagata et al., 2017; Oshima et al., 2018b). In addition, the device also solves the friction issues of the wedge-insert inside the DCB specimen reported in the literature (Kusaka et al., 1998; Isakov et al., 2019; Dillard et al., 2011; Oshima et al., 2018a).

2.3. Data reduction method

Based on the deductions of the first order beam theory described by Williams (1988) and Hashemi et al. (1990), it is possible to determine the energy release rate based on the applied moments at the end of a crack, as shown in Fig. 5. For this case, the crack is located in the mid-plane between the upper and lower sections of the beam. The load is considered to be applied centred with the mid-plane of the beam arms of the specimen. In this way, the non-linear effects due to large displacements are minimised during the analysis. Fig. 5 shows how the crack grows from point O (XW) to point O' (YZ), with an increment of delamination length Δa with respect to the initial crack length a. The upper arm is loaded with a moment M_1 and the lower arm with a moment M_2, and the uncracked portion has a bending moment $(M_1 + M_2)$.

The total energy release rate may be expressed as

$$G_{\mathrm{I}} = \frac{3}{4Eb^2h^3}\left[8{M_1}^2 + 8{M_2}^2 - \left(M_1 + M_2\right)^2\right] \tag{1}$$

where b is the width, h is half of the specimen thickness and E is the flexural modulus of the laminate for an arbitrary stacking laminate or the axial modulus of the laminate for the case of unidirectional material. Since the total energy release rate of Eq. (1) is the sum of modes I and II, it must be partitioned to obtain the mode I component (Williams,

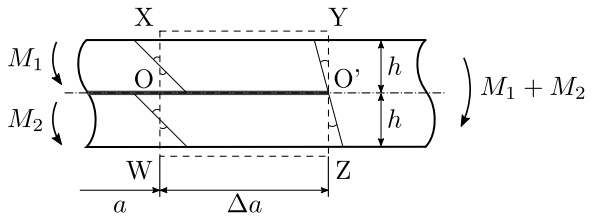

Fig. 5. Delamination geometry and loaded crack tip contour.

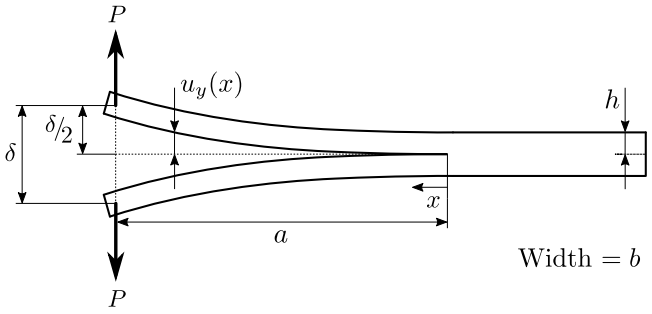

Fig. 6. Mode I double cantilever beam (DCB) configuration.

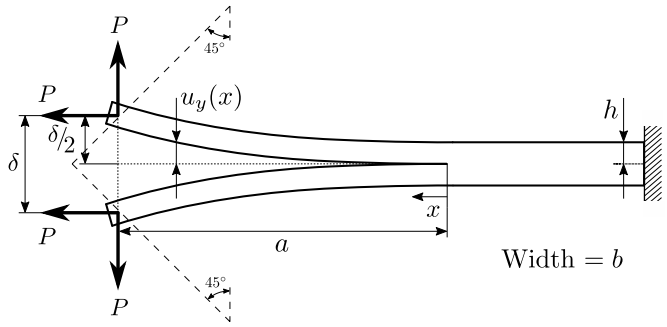

Fig. 7. Mode I guided double cantilever beam (GDCB) configuration.

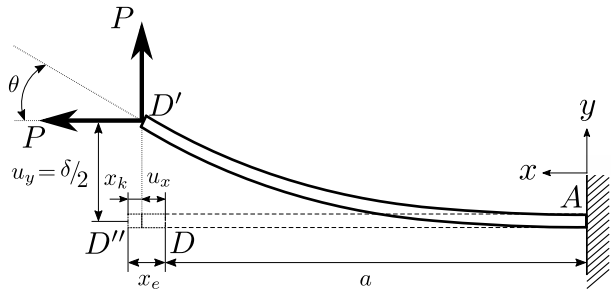

Fig. 8. Cantilever beam configuration subjected to an opening load and a tensile axial load.

1988). Pure mode I implies that the moment applied in both arms is the same, but in opposite directions. Therefore, Eq. (1) yields to

$$G_{\mathrm{I}} = \frac{6\left(M_2^2 + M_1^2\right)}{Eb^2h^3} \tag{2}$$

In the DCB mode I test configuration in Fig. 6, the bending moments are $M_2 = -M_1 = Pa$, so the expression obtained is

$$G_{\mathrm{I}} = \frac{12P^2a^2}{Eb^2h^3} \tag{3}$$

For the case of the GDCB mode I test in Fig. 7, the bending moments are defined by the contribution of the opening load and the axial–tensile load $M_2 = -M_1 = Pa - P(\delta/2)$, so the expression obtained is

$$G_{\mathrm{I}} = \frac{6}{Eb^2h^3}\left[\left(Pa - P\frac{\delta}{2}\right)^2 + \left(Pa - P\frac{\delta}{2}\right)^2\right] = \frac{12P^2a^2}{Eb^2h^3}\left(1 - \frac{\delta}{2a}\right)^2 \tag{4}$$

In the previous equations, the effect of the shear force involved is considered negligible for the calculation of the energy release rate. This assumption applies for sufficiently long cracks.

Eqs. (3) and (4) are valid for cases where the load can be measured, i.e., for quasi-static testing. Nevertheless, taking into account that the signal of the load cell is not recommendable in high loading rate tests, an alternative analysis based on displacements is required. For this, it is necessary to obtain the compliance of the system, which in the case of the DCB may be deduced from the energy release rate equation in terms of the derivative of the compliance with respect to the crack length and the Eq. (3), thus obtaining that

$$C = \frac{\delta}{P} = \frac{8a^3}{Ebh^3} \tag{5}$$

In the GDCB configuration, due to the axial–tensile load, it is not easy to obtain compliance in such a way because the opening displacement (due to the opening load) is affected by the axial force and vice versa. One way to determine the compliance of the GDCB method is by studying the deflection of a cantilever beam subjected to a combined end force as shown in Fig. 8. Therefore, assuming Euler–Bernoulli beam theory, the flexural moment can be approached as

$$M(x) = EI\frac{\mathrm{d}\theta}{\mathrm{d}s} = EI\frac{\mathrm{d}^2y}{\mathrm{d}x^2} \tag{6}$$

$$M(x) = P\left(a + u_x - x\right) - P\left(u_y - y\right) \tag{7}$$

where $M(x)$ is the equivalent bending moment applied at the arbitrary cross section, with a transverse load equal to the axial–tensile load P, x is the direction along the undeflected beam axis, y the transverse direction, a is the crack length (assumed as the length of the beam), θ is the angular deflection, and $\mathrm{d}\theta/\mathrm{d}s$ is the change rate of the angular deflection along the beam. E is the flexural modulus, I is the inertia moment, and u_x and u_y are the axial and transverse deformations at the end-edge of the arm.

The solution for Eqs. (6) and (7) was defined by Awtar et al. (2006) as approximations by inverse linear expressions to the hyperbolic functions solution. This solution captures the effects of load-stiffening and elastokinematic non-linearities in a simple beam subjected to end forces. The force equilibrium condition is applied in the deformed configuration of the beam, where the axial–tensile load contributes to the bending moments. The axial displacement u_x is comprised of two components: a purely elastic component x_e resulting from the elastic stretching of the beam, and a bending component x_k that results from the conservation of beam arc-length, as represented in Fig. 8. Liu and Yan (2017) summarised the solution for displacements of a simple beam subjected to end forces from Awtar et al. (2006), and the resulting displacement relationship in terms of the load and the flexural stiffness for the beam analysis is

$$\frac{u_y}{a} = \frac{\delta}{2a} \approx \frac{5Pa^2}{15EI + 6Pa^2} \tag{8}$$

Thus, reorganising the terms in Eq. (8), the compliance of the GDCB method can be described as

$$C = \frac{\delta}{P} \approx \frac{8a^3}{Ebh^3}\left(1 - \frac{3\delta}{5a}\right) \tag{9}$$

Using the expression of the compliance in Eq. (9), which is a function of δ and a, to obtain the value of the force P in function of the other parameters and substituting in Eq. (4), a displacement-based equation for the energy release rate can be found.

$$G_{\mathrm{I}} = \frac{3Eh^3\delta^2}{16a^4}\left[\frac{\left(1 - \frac{\delta}{2a}\right)^2}{\left(1 - \frac{3\delta}{5a}\right)^2}\right] \tag{10}$$

The previous analysis of the simple beam theory equations assumes that at the crack tip the compliance is zero (Eqs. (5) and (9)). However, some deflection and rotation at the crack tip has been proved to exist (Hashemi et al., 1990). Then, the rotation of the arms at the crack tip is modelled by adding a length χh to the crack length, defining an effective crack length $a_e = a + \chi h$, where χ is a constant given by the elastic properties of the material as described in Hashemi et al. (1990). Then, the corrected expression for the mode I energy release rate using the GDCB method is

$$G_{\mathrm{I}} = \frac{3Eh^3\delta^2}{16\left(a_e\right)^4}\left[\frac{\left(1-\frac{\delta}{2a_e}\right)^2}{\left(1-\frac{3\delta}{5a_e}\right)^2}\right] \tag{11}$$

Furthermore, corrections for large displacements and/or end block corrections might be necessary in accordance with ISO 15024:2001 (2001), and as reported by Williams (1987).

2.3.1. Correction for high loading rates

When the GDCB test is performed under high loading rates, the kinetic energy of the system may play an important role during the analysis. The transition time threshold criterion proposed by Medina et al. (2021), based on the relation between the kinetic and elastic energies, can be used to determine if the contribution of the kinetic energy is relevant for the analysis of the mode I interlaminar fracture toughness or not. For the cases where the kinetic energy plays a relevant role, its contribution to G_I can be calculated from the kinetic energy of a cantilever beam with a lumped mass m at the free end. Due to the complex solutions and the need for numerical methods to compute the real contribution of the kinetic energy, a simplified approximate solution can be used instead. Based on the work done by Blackman et al. (1996), using the simple beam theory and assuming the static displacement profile of a cantilever beam with a transverse loading, the kinetic energy can be expressed as

$$U_{\mathrm{k}} = 2\left[\frac{1}{2}\int_0^a \rho bh\left[\dot{u}_y\left(\frac{3ax^2-x^3}{2a^3}\right)\right]^2 \mathrm{d}x\right] + 2\left[\frac{1}{2}m\left(\dot{\delta}/2\right)^2\right] \tag{12}$$

$$\frac{\mathrm{d}U_{\mathrm{k}}}{\mathrm{d}a} = \frac{33\rho bh\dot{\delta}^2}{560} = \frac{33Ebh}{560}\left(\frac{\dot{\delta}}{c_{\mathrm{o}}}\right)^2 \tag{13}$$

where $c_{\mathrm{o}} = (E/\rho)^{1/2}$ is the longitudinal wave propagation velocity in the material. Finally, the displacement-based expression for the G_I of the GDCB method at high loading rates can be expressed as

$$G_{\mathrm{I}} = \frac{3Eh^3\delta^2}{16\left(a_e\right)^4}\left[\frac{\left(1-\frac{\delta}{2a_e}\right)^2}{\left(1-\frac{3\delta}{5a_e}\right)^2}\right] - \frac{33Ebh}{560}\left(\frac{\dot{\delta}}{c_{\mathrm{o}}}\right)^2 \tag{14}$$

2.4. Finite element model for design and validation

The aim of the simulations was to study the accelerations and stresses of the tool when submitted to high loading rates and to use the results in the design process. The simulations were mainly focused on the grips, in particular the pins, since they are the weakest but most loaded parts of the test system. The pins transfer the entire load from the actuator to a small contact area with the guidance plates and then, finally, to the specimen. The grips are small in size to reduce the inertia effects on the end-edges of the specimen arms and to avoid inducing non-linear effects when introducing the load onto the specimen.

A three-dimensional model of the GDCB specimen was defined using the commercial software Abaqus™/Explicit (Dassault Systèmes Simulia Corp., 2014). The composite specimen was modelled using solid elements with incompatible modes (C3D8I) to capture the bending response resulting from the large displacements, thus avoiding the shear-locking phenomena. Since the delamination must be modelled, zero-thickness cohesive elements COH3D8 were added to capture the onset of delamination and propagation. The cohesive constitutive behaviour considered was the Traction–Separation law available in Abaqus, where the delamination onset is captured based on a quadratic stress criterion, and the mixed-mode energy-based approach proposed by Benzeggagh and Kenane (1996) was used for propagation.

The GDCB specimen modelled had an initial crack length a_{o} = 92.5 mm, arm thickness h = 1.5 mm, length l = 250 mm, and width b = 20 mm. The specimen was assumed as unidirectional with all fibres parallel to the direction of the crack growth. The material used for the simulations was a unidirectional Hexply AS4/8552 CFRP composite, with the following elastic properties (Soto et al., 2018): E_1 = 128 GPa; $E_2 = E_3$ = 7.63 GPa; $G_{12} = G_{13}$ = 4.358 GPa; $\nu_{12} = \nu_{13}$ = 0.35 and ν_{23} = 0.45. The interface material properties used are (Soto et al., 2018): G_{Ic} = 0.28 N/mm; G_{IIc} = 0.79 N/mm; τ_{I} = 26 MPa; τ_{II} = 78.4 MPa and η = 1.45.

A refined mesh of the model was used in the delamination propagation zone with biased transition from fine to coarse mesh away from the crack tip, as shown in Fig. 9. The Fracture Process Zone (FPZ) and the appropriate element size in the direction of crack propagation were defined based on the approach proposed by Soto et al. (2016). The corresponding length of the FPZ for pure mode I propagation was 1.21 mm and the element size selected was 0.3 mm from the crack tip until the end of a propagation length, thus ensuring a minimum of three cohesive elements used to discretise the interlaminar FPZ. A maximum element size of 1.5 mm was used at the fixed end of the specimen. An element size of 0.375 mm was defined in the width and the through-thickness directions of the whole specimen.

The grips were modelled using hexahedron solid elements C3D8R for the pins and the central body of the grip, and tetrahedron solid elements C3D4 for the curved transition region between the pins and the central body, as shown in Fig. 10.

For the main body of the GDCB tool, the two plates with guidance profiles were modelled through surface profiles and rigid elements type R3D4 with an element size of 0.3 mm. Then, using a rigid body motion, the three previously identified zones: acceleration zone, transition zone and opening zone (constant velocity zone) were simulated. A first step was used to perform the acceleration stage until reaching the desired velocity, i.e., the acceleration zone. A second step applied constant velocity for the transition and opening zones. Velocities up to 15 m/s of the actuator were considered in different simulations to check all the possible loading rates that the servo-hydraulic tester can achieve. All the displacements at the end of the specimen were constrained, while the arms were linked to the grips by a tie constraint definition. Contact constraints between the rigid bodies of the guidance surfaces and the pins of the grips were defined. Fig. 11 shows the boundary conditions of the FE model.

2.5. Results of the FE modelling

The results of the simulations showed that the critical moment of the test is when the grips pass through the transition zone, i.e., from the acceleration zone, with no opening, to the constant velocity opening zone. It is in this transition zone that the opening force starts to appear, subjected to a change in direction. It is also in this zone when contact between loading pins and guide is intensified and even small impacts occur (Fig. 12). In order to achieve tolerant stresses in the grips, their design underwent several transformations. In fact, the final design of the grips uses titanium, thanks to its low density (titanium is around 1.8 times lighter than steel), to reduce inertial effects while ensuring a sufficiently high yield strength (1100 MPa for titanium and 1300 MPa for steel).

Apart from the analysis of stress in the pins of the grips as the most critical parts, it was also necessary to assess the performance of the guidance profiles and the specimen. In the profiles, the stresses were equal to those reported for the case of titanium pins (Fig. 12b). However, the inertia effects are not problematic for the guidance plates

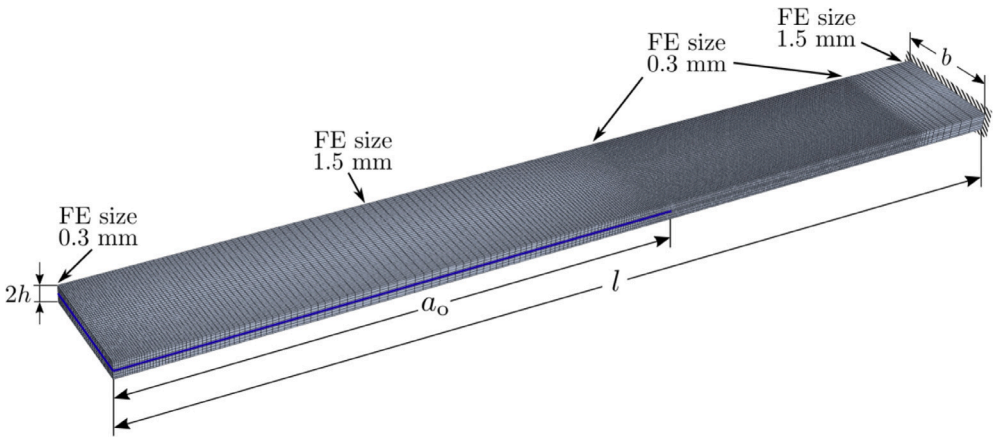

Fig. 9. Specimen mesh.

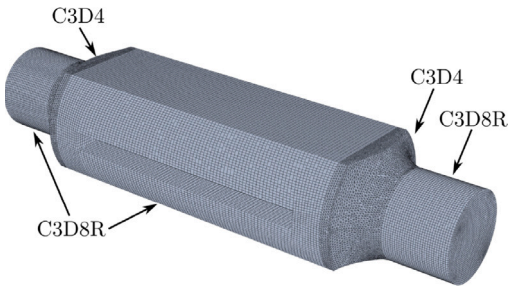

Fig. 10. Grip mesh and element types used.

as these are made of tool steel which has a higher strength than titanium. Thus, contact stresses should not cause any problem in the guiding profiles. For the specimen, there was a concern about the bending behaviour of the arms and the stresses in the region of the connection with the grips, since it is possible to overload the arms and provoke their premature failure. Following the analysis, it was observed that even for the critical loading rate of 15 m/s, the stresses in the specimen arms were low and handleable by typical composite materials.

Fig. 13 shows the opening velocity from a simulation with a tester velocity of 15 m/s. This graph validates the method and its expected behaviour, presenting an increase in the opening velocity due to the acceleration in the transition zone and reaching a constant velocity at the opening zone. However, the opening velocity increases when crack propagation begins due to the inertia effect. Although the opening velocity experiences a small increase, it can be considered as a constant value. In addition, in accordance with the design, crack propagation starts once the opening zone is reached.

3. Experimental campaign for validation and characterisation

In this section an experimental testing campaign is performed. Initially, the results of quasi-static DCB and GDCB tests with woven CFRP specimens are compared to assess and validate the proposed test method. Then, additional tests with the GDCB tool using the same material are carried out to assess its performance under high loading rate conditions.

3.1. Material and specimen geometry

The woven composite material used in this study combined the carbon fabric type G0926 (5HS, 6 K, 370 gsm) produced by Hexcel® with the HexFlow® RTM6 mono-component epoxy system using the Resin Transfer Moulding (RTM) process. The composite material has the following elastic properties (González et al., 2014): $E_{11} = 59.54$ GPa; $E_{22} = 54.95$ GPa; $G_{12} = 5.21$ GPa; and $\nu_{12} = 0.03$.

An 8-ply 400 × 300 mm^2 plate with all layers oriented in the same direction was manufactured with a 400 × 120 mm Teflon film placed at the mid-plane of one end to generate the starter crack. The stacking sequence of each of the two arms of the specimen is $[0]_4$. The specimens were cut from the plate using a diamond blade. The longitudinal edges of the specimens were polished with sandpaper of different grain sizes and coated with white spray paint to facilitate optical tracking of the crack propagation. The resulting average specimen thickness was 2.925 mm. This thickness corresponds to the mean value of cured specimens, counting six measures per specimen at different locations with a thickness variation within the limits established by the DCB standard (ISO 15024:2001, 2001). The specimen's dimensions and preparation were kept the same for the two test configurations: DCB and GDCB. The in-plane dimensions of the final samples were 270×20 mm^2.

The specimen length was selected to ensure the initiation of propagation once the transition zone is finished and a constant opening velocity is reached. Two steps are required to obtain the crack length and the opening displacement that fulfil the requested conditions. First, by using the analytical expression from Eq. (11) and assuming an expected value of the fracture toughness, an initial value of the crack length is obtained when the crack propagation starts for a defined opening displacement (value selected to be in the opening zone). Then, a trial GDCB test is performed to check if the selected crack length fulfils the condition of crack propagation only occurring in the constant opening velocity zone. Moreover, this trial test allows for any form of failure in the arms of the specimens due to excessive bending or low stiffness occurring to be assessed. In this case, based on an estimation of the expected fracture toughness, it was determined that the initial length of the crack is 105 mm long from the edge of the specimens. Before clamping the specimens to the testing machine, the cracked regions were carefully opened manually and the Teflon sheet was removed. As recommended by the DCB standard (ISO 15024:2001, 2001), all pre-cracks were extended a few millimetres using the DCB set-up to avoid any influence of resin-rich pockets originated at the edge of the Teflon tape. Once the specimens were placed into the grips, the initial crack length was around 115 mm for the DCB and 105 mm for the GDCB. Although the crack length of the DCB specimens is longer than the one specified in the DCB standard (ISO 15024:2001, 2001), it was selected to obtain load–displacement curves in the similar range as those expected in the GDCB test.

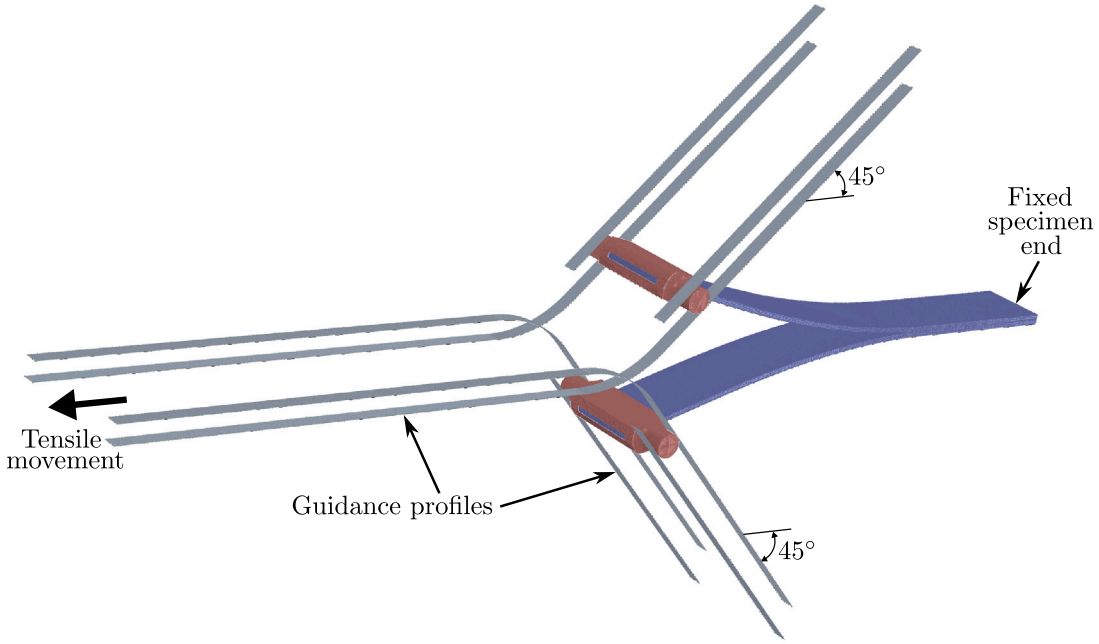

Fig. 11. FE model of the GDCB guides, specimen and grips with the applied boundary conditions.

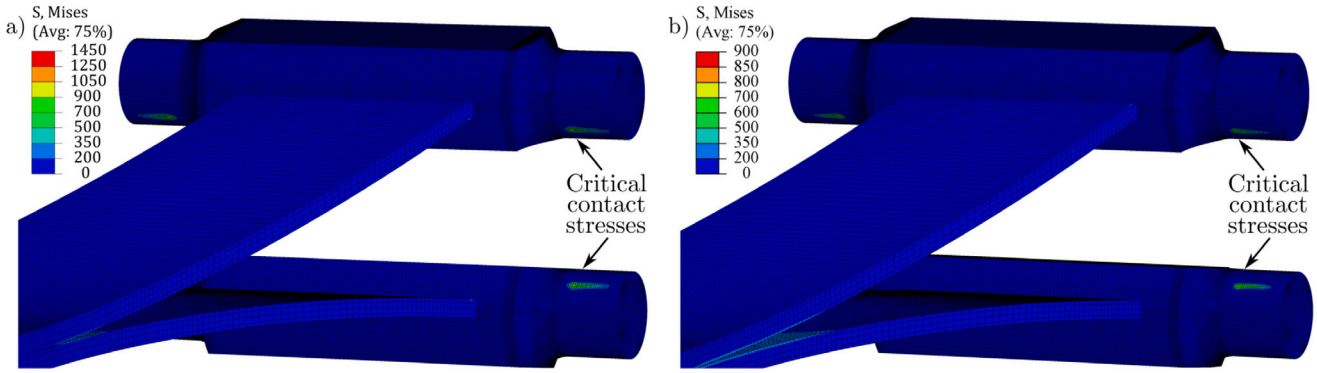

Fig. 12. Stress field in the grips in the transition zone at 15 m/s tester velocity for (a) steel grips and (b) titanium grips (stress values in MPa).

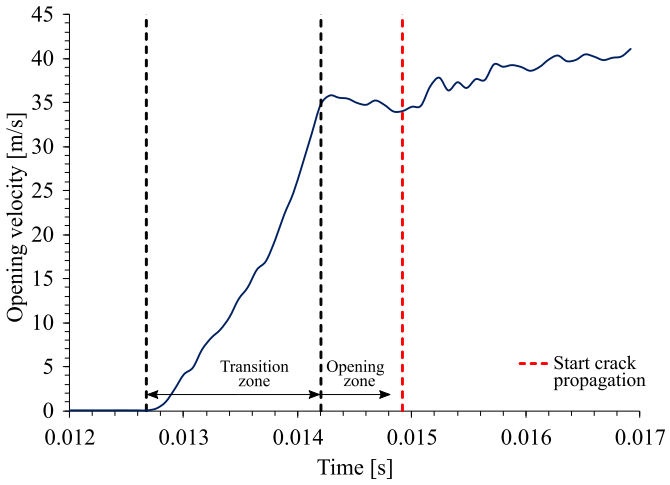

Fig. 13. Opening velocity vs time from the simulation at 15 m/s tester velocity.

3.2. Set-up for the quasi-static test validation

The quasi-static tests were performed under laboratory conditions. An electromechanical screw-driven MTS machine equipped with a 5 kN load cell was employed to load the specimens for both DCB and GDCB tests, employing a constant cross-head velocity of 5 mm/min. In addition to the own data acquisition system of the testing machine to record load and displacement, a set of two cameras was used to track the displacement at the load-application point, and to monitor the crack propagation, as shown in Fig. 14 (not included in the picture for the DCB test, Fig. 14a). Camera 1 was used to track the grips and Camera 2 the crack tip location. The displacement at the load-application point was tracked optically using markers placed at the pins in the specimen grips. For the DCB tests, the cameras recorded images at 1 fps with a resolution of 2200 × 2200 pixels. For the GDCB tests, the cameras recorded images at 3 fps with a resolution of 2048 pixels along the loading direction, and 328 pixels along the transverse direction for Camera 1 and 2048 × 2048 pixels for Camera 2. The lighting conditions during testing were set in such a way that a sharp contrast between the white specimen surface and the background was obtained. Fig. 15 shows a photo frame for the set of two cameras used in the GDCB test.

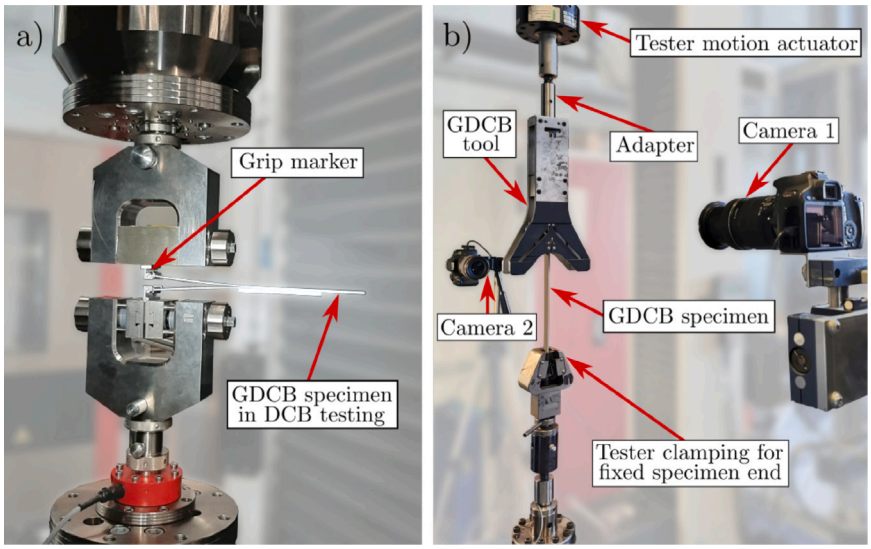

Fig. 14. Set-ups for the quasi-static testing of (a) the DCB and (b) the GDCB (rotated 180° with respect to the usual orientation).

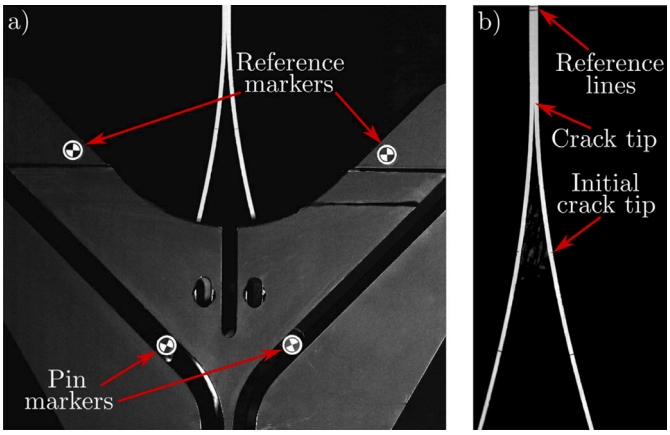

Fig. 15. Photo frames from (a) Camera 1 and (b) Camera 2 for the image analysis of the GDCB.

Although the DCB quasi-static tests were performed based on the standard ISO 15024:2001 (2001), some modifications such as the initial crack length and the length of the specimen were carried out. Additionally, the same data reduction process with the image analysis was used in the DCB to validate the data acquisition and data reduction methods for the GDCB. The grip markers and the two cameras were also used for the DCB tests, requiring the use of the same grip system as the GDCB and using an additional part to obtain the hinge behaviour over the pins of the grips.

All the images taken with the two cameras were post-processed using in-house Matlab scripts/algorithms. The script for Camera 1 analyses all the image frames from this camera to determine the current position of the pin and the reference markers. Then, the opening displacement is obtained as the distance between the two loading pins, as seen in Fig. 16a. The reference markers are used as set points for the pin markers and as a control for the conversion from pixels to millimetres. Finally, the opening velocity can be calculated using the testing time. A second Matlab script is used to determine the current position of the crack tip along the test by processing the images taken with Camera 2. First, the longitudinal inner edge of each specimen arm is detected, as shown in Fig. 16b. Next, a polynomial expression is adjusted to each inner arm edge by a curve fitting process. Finally, the crack tip is detected by the intersection of the two polynomial curves, as shown in Fig. 16c. In Fig. 16c, two different crack tips are shown: the crack tip from the image analysis, which is the one detected by the pixel analysis, and the predicted crack tip, which is the one from the curve fitting process. The pixel analysis is underestimated and inaccurate since it relies on the optical resolution of the system, without considering the nearby deflection of the arms. Therefore, the useful crack tip is the one defined by the curve fitting process.

3.3. Results and discussion for the quasi-static validation

Fig. 17 shows the experimental and analytical load–displacement curves for both the DCB and GDCB tests. The experimental curves do not start at zero displacement because the test is initiated with the arms slightly open, and therefore elastically preloaded. From this figure, a clear stick–slip behaviour present in the experimental DCB curves can be seen, while the experimental GDCB curves have a noisy behaviour that may conceal the stick–slip drops. The noise in these curves can be explained by the contact between the pins and the guidance plates in the GDCB method. As will be commented on in more depth later, the effect of this noise on the GDCB test is more important for quasi-static and low-velocity conditions. Due to stick–slip, the pre-cracking process of the DCB and GDCB specimens resulted in a crack propagation greater than the 3 to 5 mm defined by the standard, with a remarkable difference between the initial crack length of the specimens used for the GDCB test. This is why the elastic stiffness of both GDCB curves shown in Fig. 17 differs considerably between them. The analytical curves were obtained from a mean value of the initial crack length for both cases. In both cases, the experimental curves show a high dispersion during propagation mainly due to the stick–slip behaviour. Even so, the experimental curves follow the same trend as the analytical ones from Eqs. (3) and (4).

Additionally, in Fig. 17 the effect of the axial load involved in the GDCB method when compared to the DCB can also be seen. This axial load affects the compliance, as seen by comparing Eqs. (5) and (9), resulting in a non-linear increment in the elastic curve of the chart, increasing the maximum load and shifting the crack propagation curve. The figure shows the analytical curves with the loading, propagation up to the same crack length for both methods, and unloading stages. It is worth mentioning that although both curves show different trends in stiffness, maximum load and propagation curve, the areas between the three curves for each specimen type (shaded/coloured areas in Fig. 17) are exactly the same and correspond to the dissipated energy during the crack growth process, i.e., the same fracture toughness.

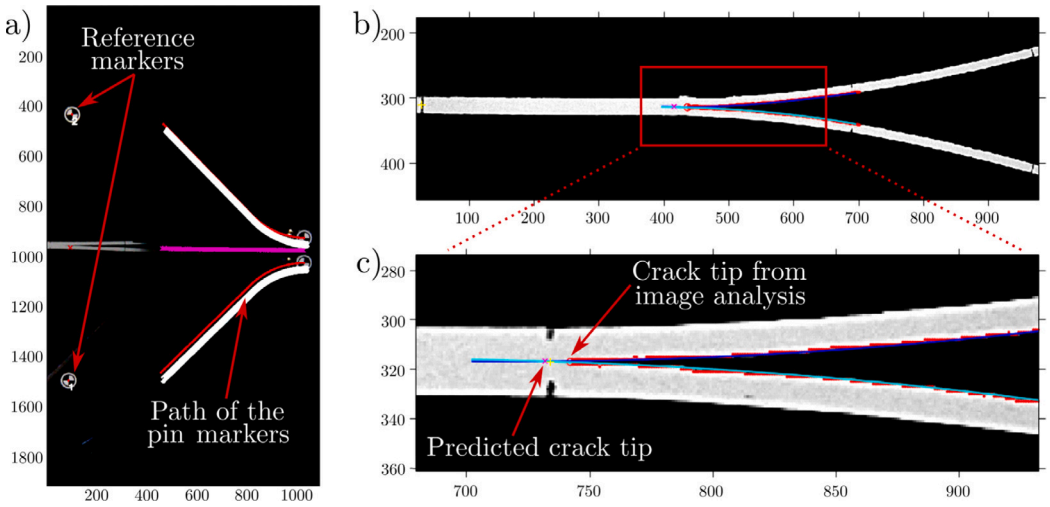

Fig. 16. Matlab script images for the analysis of the GDCB from (a) Camera 1, (b) Camera 2 and (c) close-up of the Camera 2 analysis (axes units in pixels).

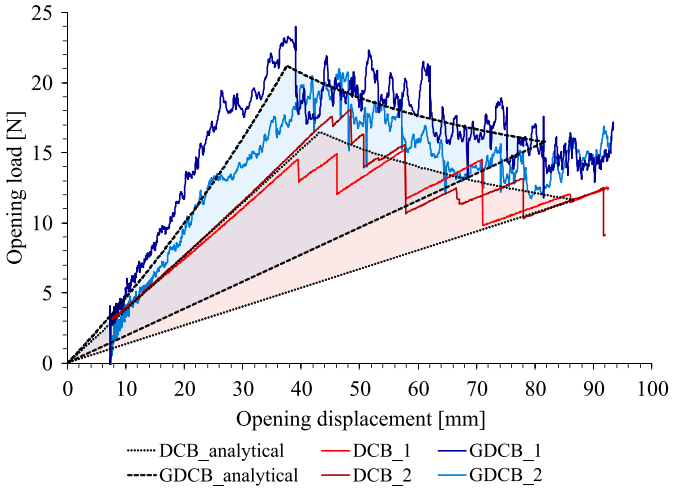

Fig. 17. Load–displacement curves for DCB and GDCB tests. Coloured areas correspond to theoretical dissipated energy in each case for comparison purposes.

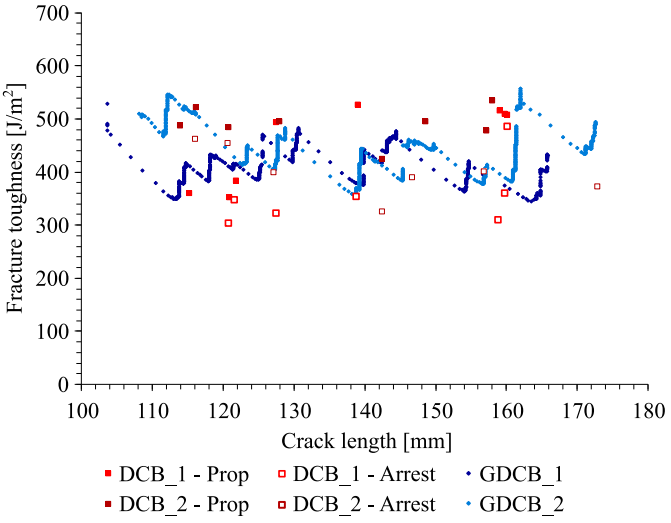

Fig. 18. Quasi-static mode I fracture toughness for quasi-static DCB and GDCB tests.

Fig. 18 shows the variation in the mode I interlaminar fracture toughness vs the crack length for the DCB and GDCB tests. While for the GDCB a higher number of data reduction points can be used and a more continuous evolution of G_Ic can be determined, only the discreet propagation and arrest points are obtained for the DCB case. Despite this, in both cases the large scatter of the fracture behaviour of the material can be clearly seen. This is due to the stick–slip crack propagation behaviour (see Fig. 17). Despite the fracture behaviour observed and the associated large scatter, the values of the fracture toughness are in the same range for both test methods, thus validating the GDCB method for mode I delamination testing.

3.4. Testing set-up at intermediate/high loading rates

The aim of this testing campaign was to demonstrate the performance of the tool when submitted to intermediate/high testing velocities. The objective of these tests was to verify whether a symmetrical opening of the specimen arms was obtained under dynamic conditions and if the loading rate had any effect on the fracture toughness of the material tested. Accordingly, a series of experimental GDCB tests were carried out, using the same material and specimen dimensions as in the quasi-static validation.

The tests were performed under laboratory conditions using an Instron VHS servo-hydraulic high loading rate machine. As noted in Section 2.2, during the tests special care was taken to ensure that crack propagation took place after the transition zone of the guiding profiles.

As explained earlier, measuring the force in high-velocity experiments is not recommended. This is why the test set-up was prepared for a data reduction process based on image analysis. The set-up, as shown in Fig. 19, consists of a set of two cameras: one to track the displacement at the load application points in the specimen (Camera 1), and the other to monitor the crack length growth (Camera 2). The cameras used were two Photron Fastcam SA-Z high-speed cameras with Tokina 100 mm f2.8 macro lenses. One position signal of the machines was selected and used as the trigger for activating the high-speed camera system. The lighting conditions during testing were set in such a way that a sharp contrast between the white specimen surface and the background was obtained using an in-house LED lighting system of more than 70,000 lumens (Artero-Guerrero et al., 2015). In addition, the images taken during the tests were post-processed using the Matlab scripts/algorithms, as explained in Section 3.2.

The tests were conducted at four different loading velocities of the tester's actuator: 0.1, 1, 3, and 10 m/s (tester loading rates from now on). Three specimens per loading rate were tested. The frame rates and

Table 1
Frame rates and resolution of the high-speed cameras for the intermediate/high loading rates testing.

Tester loading rate [m/s]	Data acquisition rate [fps]	Resolution Cam 1 [pixels]	Shutter Cam 1 [s]	Resolution Cam 2 [pixels]	Shutter Cam 2 [s]
0.1	2000	1024 × 1024	1/80000	1024 × 1024	1/50000
1	15000	1024 × 1024	1/80000	1024 × 1024	1/50000
3	30000	896 × 736	1/80000	640 × 1024	1/50000
10	30000	896 × 736	1/80000	640 × 1024	1/50000

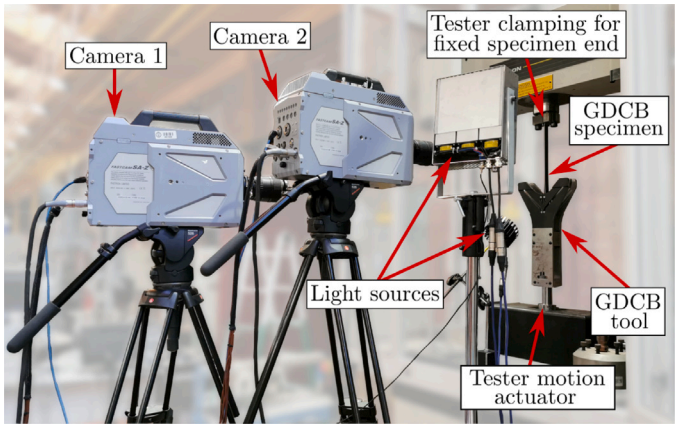

Fig. 19. GDCB set-up for high loading rate testing.

resolution of the cameras used for the different velocities are shown in Table 1. By modifying the required window for each camera, the resolution of the cameras was adjusted with the increase of the test loading velocity to obtain higher fps and be able to capture the crack propagation.

3.5. Results and discussion of the intermediate/high loading rate tests

The results of the mode I interlaminar fracture toughness for intermediate/high loading rates are shown in Fig. 20 using Eq. (14). The same stick–slip fracture behaviour of the material observed for the quasi-static cases can also be seen here. However, when increasing the loading rate, the stick–slip events are reduced, both in number and amplitude. A similar observation has already been reported by Blackman et al. (1996, 2009). Although there is significant scatter in the data, similar trends can be observed for all cases.

To assess the effect taking into account the kinetic energy has on determining the interlaminar fracture toughness energy, a comparison between the data reduction using Eq. (11) (without kinetic energy effects) and Eq. (14) (with kinetic energy effects) can be established. Fig. 21 shows this comparison for the cases of 3 and 10 m/s. Notice that, at 3 m/s or smaller, the contribution of the kinetic energy to the dynamic fracture toughness is relatively low; in fact negligible for the cases of 0.1 and 1 m/s (not included in the figure for simplicity). However, for a loading rate of 10 m/s this contribution cannot be neglected. In fact, the value of G_{IC} without taking into account the kinetic term is around 15% higher. This might explain why studies available in the literature report an inaccurate value of the interlaminar fracture toughness at medium/high loading rates.

It is possible to use the numerically-based expression for the transition time proposed in Medina et al. (2021) to assess which tester loading rates fulfil the time-based threshold criterion ($t_f > 2.03\ t_\tau$) so a quasi-static data reduction scheme can be used. With t_τ being the transition time, and t_f the time to fracture (i.e., the time of the crack propagation start, for the specimen dimensions and material used in these tests), a transition time of 1.8 ms is obtained. Thus, the time to fracture should be $t_f > 3.6$ ms. For the tester loading rates considered in this case, 0.1, 1, 3 and 10 m/s, the corresponding times to fracture are 200, 24, 7.3 and 2 ms, respectively. Therefore, according to this criterion, only the tests at 10 m/s cannot be treated using a quasi-static data reduction scheme. Besides, even in the case of a tester loading rate of 3 m/s, where the kinetic energy contribution over the fracture toughness is perceptible as shown in Fig. 21, the effect is minimum and can be neglected.

Table 2
Mode I fracture toughness results for the quasi-static testing of the DCB and the GDCB, and for intermediate/high loading rates testing using the GDCB method.

			G_{Ic} [J/mm^2]
DCB	–	quasi-static	422 ± 57
GDCB	–	quasi-static	430 ± 45
GDCB	–	0.1 m/s	402 ± 70
GDCB	–	1 m/s	420 ± 88
GDCB	–	3 m/s	388 ± 92
GDCB	–	10 m/s	489 ± 105

Table 2 summarises the mean values of the interlaminar fracture toughness for the quasi-static, DCB and GDCB, and intermediate/high loading rate GDCB tests. No clear effect of the loading rate can be seen up to 3 m/s tester velocities. As previously explained, there is a high scatter in all the cases, as indicated by the large standard deviation values for each case.

The variation in the opening velocities of the arms with respect to the loading velocities for the GDCB device are shown in Fig. 22. The results of the three specimens per loading rate are shown. All the curves present the same overall behaviour: initial velocity increase with constant slope/acceleration, short transition zone and horizontal/plateau in the constant opening velocity. Once the specimen has reached the velocity plateau, the curve remains smooth until the crack propagation begins, with a variation due to the propagation and the stick–slip effect being seen. As can be observed in the figure, the value of the crack opening velocity in the opening zone is fairly constant and equal to 2.5 times the corresponding tester loading rate. From Fig. 22, it is important to highlight the smooth velocity plateau at high loading rates, i.e., 10 m/s of the tester or around 25 m/s for the opening velocity of the arms. The oscillations in the crack opening velocity, especially in the opening zone, are due to the stick–slip fracture behaviour of the material. These oscillations are less evident as the loading rate is increased.

Fig. 23 summarises the results of the fracture toughness for each of the four velocities tested in terms of the crack propagation velocities. This figure is obtained by considering the mean value of the fracture toughness and the associated standard deviation for different values of crack propagation velocities for each tester loading rate. The results present an important scatter, increasing with the increase in the loading rate. Due to the stick–slip behaviour present in the tests, a wide range of crack propagation velocities can be achieved for each one of the tester loading rates. For the tester loading rate of 0.1 m/s, crack propagation velocities up to 65 times the tester velocity were reached; for 1 and 3 m/s up to 20 times; and for 10 m/s almost 10 times. Therefore, the higher the tester loading rate, the fewer stick–slip events, and the lower the crack propagation velocity reached. Despite the scatter, the mean values of the fracture toughness for the tester loading rates of 0.1, 1 and 3 m/s are similar, thus making it possible to conclude that

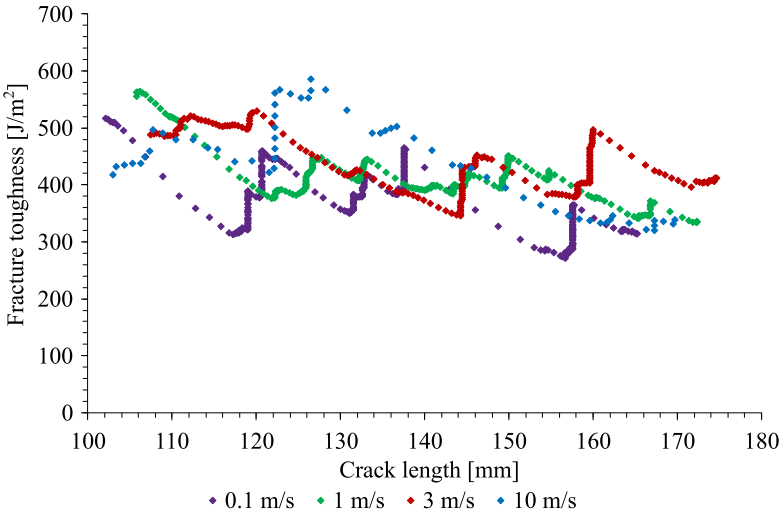

Fig. 20. Mode I fracture toughness for the intermediate/high loading rate GDCB tests.

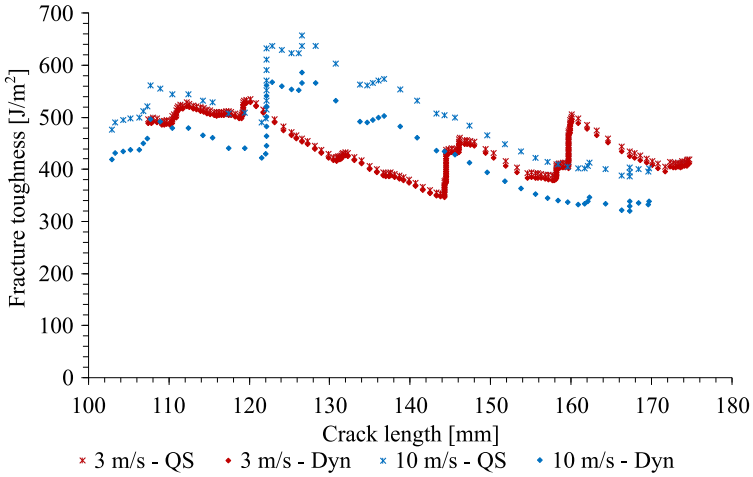

Fig. 21. Effect of the kinetic energy for the GDCB tests (QS corresponds to Eq. (11), without kinetic energy effects and Dyn corresponds to Eq. (14), with kinetic energy effects).

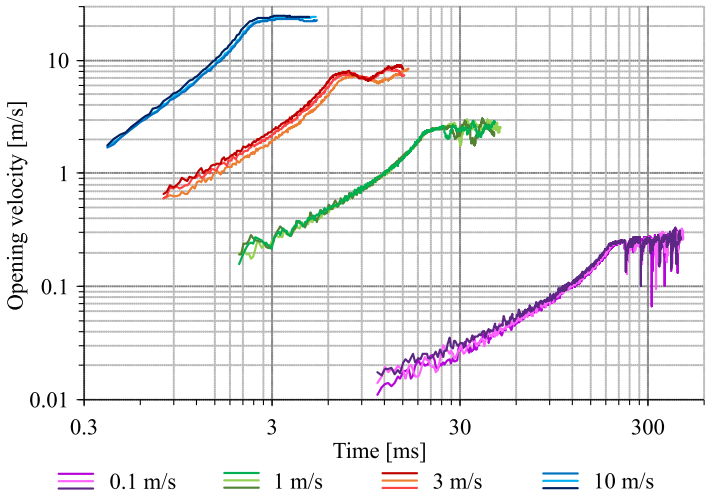

Fig. 22. Opening velocities vs time for the loading velocities of the GDCB tests.

for these loading rates and material used there is no effect on the interlaminar fracture toughness. However, for the tests at 10 m/s, the fracture toughness values are significantly higher, as seen in Fig. 23. Although these results seem to indicate that the loading velocity has an effect on the interlaminar fracture toughness of the material, there are some considerations to take into account. The dynamic correction of Eq. (14) is based on the beam theory of a DCB specimen and does not account for the axial load effect. Besides, non-linear effects can be

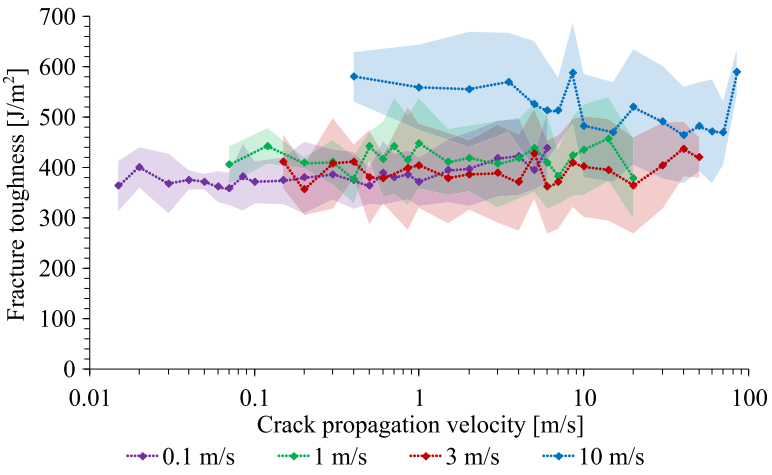

Fig. 23. Fracture toughness in terms of the crack propagation velocities.

important enough at these velocities that they cannot be discarded. Therefore, the contribution to the energy release rate may be overestimated, thus necessitating an improvement in the data reduction method for high loading rates.

4. Conclusions

A novel test method for the interlaminar fracture toughness in mode I loading at intermediate and high loading rates has been presented. The proposed device solves the issues of asymmetrical loading when using DCB at high loading rates, and not requiring adhesive joints allows for easy reuse. The GDCB method has been validated under quasi-static loading by comparing it with DCB tests. An experimental test campaign under intermediate/high loading rates to assess the performance of the device has been performed. From the results, it can be concluded that the GDCB method is appropriate for dynamic fracture toughness testing in composites. For the material used, the loading rates show no clear effect on the interlaminar mode I fracture toughness up to 3 m/s tester loading rate. However, at 10 m/s there is an effect and what must be assessed is whether this is due to a sensitivity of the material property or an overestimation of the property by the data reduction method used. It is important to highlight that the material tested presented stick–slip behaviour and high scatter, which makes it difficult to properly assess the effect of the loading rate. A larger number of tested specimens per configuration could help to reduce this level of scatter. It has been shown that at high loading rates the contribution of the inertia effects to the calculation of the fracture toughness is significant, about 15%. Further studies using other materials and improving the data reduction method are proposed as future work.

CRediT authorship contribution statement

S.A. Medina: Conceptualization, Methodology, Software, Formal analysis, Investigation, Writing – original draft. **E.V. González:** Conceptualization, Supervision, Writing – review & editing. **N. Blanco:** Conceptualization, Supervision, Writing – review & editing. **J. Pernas-Sánchez:** Resources, Investigation, Writing – review & editing. **J.A. Artero-Guerrero:** Resources, Investigation, Writing – review & editing.

Declaration of competing interest

The authors declare the following financial interests/personal relationships which may be considered as potential competing interests: Sergio Medina reports financial support was provided by Spain Ministry of Science and Innovation. Emilio Gonzalez reports financial support was provided by Spain Ministry of Science and Innovation. Sergio Medina has patent #PCT/ES2021/070415 licensed to WO/2022/003219.

Data availability

Data will be made available on request.

Acknowledgements

The authors would like to acknowledge the financial support from the Spanish Ministerio de Ciencia, Innovación y Universidades through the projects RTI2018-099373-B-I00 and RTI2018-097880-B-I00. The first author also acknowledges the grant for doctoral studies IFUdG2017/43.

References

Aliyu, A.A., Daniel, I.M., 1985. Effects of strain rate on delamination fracture toughness of graphite/epoxy. In: Delamination and Debonding of Materials. ASTM International, 100 Barr Harbor Drive, PO Box C700, West Conshohocken, PA 19428–2959, pp. 336–336–13. http://dx.doi.org/10.1520/STP36313S.

Artero-Guerrero, J., Pernas-Sánchez, J., López-Puente, J., Varas, D., 2015. Experimental study of the impactor mass effect on the low velocity impact of carbon/epoxy woven laminates. Compos. Struct. 133, 774–781. http://dx.doi.org/10.1016/j.compstruct.2015.08.027.

ASTM D5528-13, 2013. Standard test method for mode I interlaminar fracture toughness of unidirectional fiber-reinforced polymer matrix composites. In: Standard. ASTM International, West Conshohocken, PA, http://dx.doi.org/10.1520/D5528-13.

Awtar, S., Slocum, A.H., Sevincer, E., 2006. Characteristics of beam-based flexure modules. J. Mech. Des. 129 (6), 625–639. http://dx.doi.org/10.1115/1.2717231.

Benzeggagh, M.L., Kenane, M., 1996. Measurement of mixed-mode delamination fracture toughness of unidirectional glass/epoxy composites with mixed-mode bending apparatus. Compos. Sci. Technol. 56 (4), 439–449. http://dx.doi.org/10.1016/0266-3538(96)00005-X.

Blackman, B.R.K., Dear, J.P., Kinloch, A.J., Macgillivray, H., Wang, Y., Williams, J.G., Yayla, P., 1995. The failure of fibre composites and adhesively bonded fibre composites under high rates of test. Part I Mode I loading - experimental studies. J. Mater. Sci. 30 (23), 5885–5900. http://dx.doi.org/10.1007/BF01151502.

Blackman, B.R.K., Kinloch, A.J., Rodriguez Sanchez, F.S., Teo, W.S., Williams, J.G., 2009. The fracture behaviour of structural adhesives under high rates of testing. Eng. Fract. Mech. 76 (18), 2868–2889. http://dx.doi.org/10.1016/j.engfracmech.2009.07.013.

Blackman, B.R.K., Kinloch, A.J., Wang, Y., Williams, J.G., 1996. The failure of fibre composites and adhesively bonded fibre composites under high rates of test. Part II Mode I loading - dynamic effects. J. Mater. Sci. 31 (17), 4451–4466. http://dx.doi.org/10.1007/BF00366341.

Brunner, A., Blackman, B., Davies, P., 2001. Mode I delamination. In: Moore, D., Pavan, A., Williams, J. (Eds.), Fracture Mechanics Testing Methods for Polymers, Adhesives and Composites. In: European Structural Integrity Society, vol. 28, Elsevier, pp. 277–305. http://dx.doi.org/10.1016/S1566-1369(01)80038-8.

Brunner, A.J., Warnet, L., Blackman, B.R., 2021. 35 Years of standardization and research on fracture of polymers, polymer composites and adhesives in ESIS TC4: Past achievements and future directions. Procedia Struct. Integr. 33, 443–455. http://dx.doi.org/10.1016/j.prostr.2021.10.051, 26th International Conference on Fracture and Structural Integrity.

Cantwell, W.J., Blyton, M., 1999. Influence of loading rate on the interlaminar fracture properties of high performance composites - a review. Appl. Mech. Rev. 52 (6), 199. http://dx.doi.org/10.1115/1.3098934.

Colin de Verdiere, M., Skordos, A.A., May, M., Walton, A.C., 2012b. Influence of loading rate on the delamination response of untufted and tufted carbon epoxy non crimp fabric composites: Mode I. Eng. Fract. Mech. 96, 11–25. http://dx.doi.org/10.1016/j.engfracmech.2012.05.015.

Colin de Verdiere, M., Skordos, A.A., Walton, A.C., May, M., 2012a. Influence of loading rate on the delamination response of untufted and tufted carbon epoxy non-crimp fabric composites/Mode II. Eng. Fract. Mech. 96, 1–10. http://dx.doi.org/10.1016/j.engfracmech.2011.12.011.

Dassault Systèmes Simulia Corp., 2014. Abaqus analysis user's manual. In: Abaqus Documentation 6.14. Simulia Worldwide Headquarters, Providence, RI, USA.

Dillard, D.A., Pohlit, D.J., Jacob, G.C., Starbuck, J.M., Kapania, R.K., 2011. On the use of a driven wedge test to acquire dynamic fracture energies of bonded beam specimens. J. Adhes. 87 (4), 395–423. http://dx.doi.org/10.1080/00218464.2011.562125.

Feng, W.W., Reifsnider, K.L., Sendeckyj, G.P., Chiao, T.T., Rodericks, G.L., Stinchcomb, W.W., de Vore, L., Hunston, D.L., Bascom, W.D., 1983. Effects of lay-up, temperature, and loading rate in double cantilever beam tests of interlaminar crack growth. J. Compos. Technol. Res. 5 (4), 118. http://dx.doi.org/10.1520/CTR10810J.

González, E., Maimí, P., Sainz de Aja, J., Cruz, P., Camanho, P., 2014. Effects of interply hybridization on the damage resistance and tolerance of composite laminates. Compos. Struct. 108, 319–331. http://dx.doi.org/10.1016/j.compstruct.2013.09.037.

Hashemi, S., Kinloch, A.J., Williams, J.G., 1990. The analysis of interlaminar fracture in uniaxial fibre-polymer composites. Proc. Royal Soc. Lond. Ser. A Math. Phys. Sci. 427 (1872), 173–199.

Hug, G., Thévenet, P., Fitoussi, J., Baptiste, D., 2006. Effect of the loading rate on mode I interlaminar fracture toughness of laminated composites. Eng. Fract. Mech. 73 (16), 2456–2462. http://dx.doi.org/10.1016/j.engfracmech.2006.05.019.

Isakov, M., May, M., Hahn, P., Paul, H., Nishi, M., 2019. Fracture toughness measurement without force data – Application to high rate DCB on CFRP. Composites A 119, 176–187. http://dx.doi.org/10.1016/j.compositesa.2019.01.030.

ISO 15024:2001, 2001. Fibre-reinforced plastic composites — Determination of mode I interlaminar fracture toughness, GIC, for unidirectionally reinforced materials. In: Standard. International Standardization Organization, Geneva, CH.

Jacob, G.C., Starbuck, J.M., Fellers, J.F., Simunovic, S., Boeman, R.G., 2005. The effect of loading rate on the fracture toughness of fiber reinforced polymer composites. J. Appl. Polym. Sci. 96 (3), 899–904. http://dx.doi.org/10.1002/app.21535.

Jadhav, A., 2003. High Strain Rate Properties of Polymer Matrix Composites (LSU Master's theses).

Jiang, F., Vecchio, K.S., 2009. Hopkinson bar loaded fracture experimental technique: a critical review of dynamic fracture toughness tests. Appl. Mech. Rev. 62 (6), 060802. http://dx.doi.org/10.1115/1.3124647.

JIS K 7086:1993, 1993. Testing methods for interlaminar fracture toughness of carbon fibre reinforced plastics. In: Standard. Japanese Standards Association.

Körber, H., 2010. Mechanical Response of Advanced Composites Under High Strain Rates (Ph.D. thesis). Faculdade de Engenharia - Universidade do Porto.

Kusaka, T., Hojo, M., Mai, Y.-W., Kurokawa, T., Nojima, T., Ochiai, S., 1998. Rate dependence of mode I fracture behaviour in carbon-fibre/epoxy composite laminates. Compos. Sci. Technol. 58 (3–4), 591–602. http://dx.doi.org/10.1016/S0266-3538(97)00176-0.

Liu, H., Meng, X., Zhang, H., Nie, H., Zhang, C., Li, Y., 2019. The dynamic crack propagation behavior of mode I interlaminar crack in unidirectional carbon/epoxy composites. Eng. Fract. Mech. 215, 65–82. http://dx.doi.org/10.1016/j.engfracmech.2019.05.004.

Liu, P., Yan, P., 2017. A modified pseudo-rigid-body modeling approach for compliant mechanisms with fixed-guided beam flexures. Mech. Sci. 8 (2), 359–368. http://dx.doi.org/10.5194/ms-8-359-2017.

Low, K., Teng, S., Johar, M., Israr, H., Wong, K., 2019. Mode I delamination behaviour of carbon/epoxy composite at different displacement rates. Composites B 176, 107293. http://dx.doi.org/10.1016/j.compositesb.2019.107293.

Mall, S., Law, G.E., Katouzian, M., 1987. Loading rate effect on interlaminar fracture toughness of a thermoplastic composite. J. Compos. Mater. 21 (6), 569–579. http://dx.doi.org/10.1177/002199838702100607.

Marzi, S., Rauh, A., Hinterhölzl, R.M., 2014. Fracture mechanical investigations and cohesive zone failure modelling on automotive composites. Compos. Struct. 111, 324–331. http://dx.doi.org/10.1016/j.compstruct.2014.01.016.

May, M., 2015. Numerical evaluation of cohesive zone models for modeling impact induced delamination in composite materials. Compos. Struct. 133, 16–21. http://dx.doi.org/10.1016/j.compstruct.2015.07.032.

May, M., 2016. Measuring the rate-dependent mode I fracture toughness of composites – A review. Composites A 81, 1–12. http://dx.doi.org/10.1016/j.compositesa.2015.10.033.

Medina, S., González, E., Blanco, N., 2021. Transition time threshold for Double Cantilever Beam specimens under high loading rates. Eng. Fract. Mech. 249, 107754. http://dx.doi.org/10.1016/j.engfracmech.2021.107754.

Nasuha, N., Azmi, A.I., Tan, C.L., 2017. A review on mode-I interlaminar fracture toughness of fibre reinforced composites. J. Phys. Conf. Ser. 908, 012024. http://dx.doi.org/10.1088/1742-6596/908/1/012024.

Neumayer, J.S., 2017. Characterisation and Simulation of Adhesively Bonded Joints with Laminated Adherends for Crash Applications (Ph.D. thesis). Technischen Universität München, p. 164.

Oshima, S., Ishida, H., Kusaka, T., Takeda, T., 2018a. Experimental characterization of dynamic crack growth behavior in CFRP adhesive interface. Adv. Compos. Mater. 27 (4), 397–411. http://dx.doi.org/10.1080/09243046.2017.1401336.

Oshima, S., Yoshimura, A., Hirano, Y., Ogasawara, T., 2018b. Experimental method for mode I fracture toughness of composite laminates using wedge loaded double cantilever beam specimens. Composites A 112, 119–125. http://dx.doi.org/10.1016/j.compositesa.2018.05.036.

Riezzo, M.A., Simmons, M., González, C., Sket, F., 2018. Dynamic characterization of interlaminar toughness in carbon fibre epoxy composite laminates. In: ECCM18 - 18th European Conference on Composite Materials. Athens, Greece.

Sela, N., Ishai, O., 1989. Interlaminar fracture toughness and toughening of laminated composite materials: a review. Composites 20 (5), 423–435. http://dx.doi.org/10.1016/0010-4361(89)90211-5.

Siddique, A., Abid, S., Shafiq, F., Nawab, Y., Wang, H., Shi, B., Saleemi, S., Sun, B., 2021. Mode I fracture toughness of fiber-reinforced polymer composites: A review. J. Indust. Text. 50 (8), 1165–1192. http://dx.doi.org/10.1177/1528083719858767.

Smiley, A.J., Pipes, R.B., 1987. Rate effects on mode I interlaminar fracture toughness in composite materials. J. Compos. Mater. 21 (7), 670–687. http://dx.doi.org/10.1177/002199838702100706.

Soto, A., González, E.V., Maimí, P., Mayugo, J.A., Pasquali, P.R., Camanho, P.P., 2018. A methodology to simulate low velocity impact and compression after impact in large composite stiffened panels. Compos. Struct. 204, 223–238. http://dx.doi.org/10.1016/j.compstruct.2018.07.081.

Soto, A., González, E.V., Maimí, P., Turon, A., Sainz de Aja, J.R., Martín de la Escalera, F., 2016. Cohesive zone length of orthotropic materials undergoing delamination. Eng. Fract. Mech. 159, 174–188. http://dx.doi.org/10.1016/j.engfracmech.2016.03.033.

Sun, C.T., Han, C., 2004. A method for testing interlaminar dynamic fracture toughness of polymeric composites. Composites B 35 (6–8), 647–655. http://dx.doi.org/10.1016/j.compositesb.2004.04.006.

Thorsson, S.I., Waas, A.M., Schaefer, J., Justusson, B., Liguore, S., 2018. Effects of elevated loading rates on mode I fracture of composite laminates using a modified wedge-insert fracture method. Compos. Sci. Technol. 156, 39–47. http://dx.doi.org/10.1016/j.compscitech.2017.12.018.

Tsai, J.L., Guo, C., Sun, C.T., 2001. Dynamic delamination fracture toughness in unidirectional polymeric composites. Compos. Sci. Technol. 61 (1), 87–94. http://dx.doi.org/10.1016/S0266-3538(00)00197-4.

Williams, J., 1987. Large displacement and end block effects in the 'DCB' interlaminar test in modes I and II. J. Compos. Mater. 21 (4), 330–347. http://dx.doi.org/10.1177/002199838702100403.

Williams, J.G., 1988. On the calculation of energy release rates for cracked laminates. Int. J. Fract. 36 (2), 101–119. http://dx.doi.org/10.1007/BF00017790.

Xu, S., Dillard, D., 2003. Determining the impact resistance of electrically conductive adhesives using a falling wedge test. IEEE Trans. Compon. Packag. Technol. 26 (3), 554–562. http://dx.doi.org/10.1109/TCAPT.2003.817646.

Yamagata, Y., Lu, X., Sekiguchi, Y., Sato, C., 2017. Experimental investigation of mode I fracture energy of adhesively bonded joints under impact loading conditions. Appl. Adhesion Sci. 5 (1), 7. http://dx.doi.org/10.1186/s40563-017-0087-7.